Pressure-Induced Amidine Formation via Side-Chain Polymerization in a Charge-Transfer Cocrystal

Samuel G. Dunning,[*,†] Wan Si Tang,[†,⊥] Bo Chen,[‡] Li Zhu,[§] George D. Cody,[†] Stella Chariton,[‖] Vitali B. Prakapenka,[‖] and Timothy A. Strobel[*,†]

[†]Earth and Planets Laboratory, Carnegie Institution for Science, Washington, District of Columbia 20015, United States

[‡]Donostia International Physics Center, Paseo Manuel de Lardizabal, 4, 20018 Donostia-San Sebastian, Spain; IKERBASQUE, Basque Foundation for Science, Plaza Euskadi 5, 48009 Bilbao, Spain

[§] Physics Department, Rutgers University-Newark, 101 Warren Street, Newark, NJ 07102, United States

[‖] Center for Advanced Radiation Sources, The University of Chicago, Chicago, Illinois 60637, United States

Compression of small molecules can induce solid-state reactions with products that are difficult or impossible to obtain through solution-phase synthesis. Of particular interest is the topochemical-like reaction of arenes to produce polymeric nanomaterials rich in sp3 carbon. However, high reaction onset pressures and poor control over high-pressure reaction selectivity remain significant challenges to be addressed. Herein, the incorporation of electron withdrawing/donating groups into π-stacked arenes is proposed as a strategy to reduce reaction barriers and onset pressures. Charge transfer cocrystals represent systems with optimal π-stacking and reduced energy barriers for intermolecular cycloaddition reactions, however, competing side-chain reactions between functional groups must also be considered. For the case of a diaminobenzene:tetracyanobenzene cocrystal, amidine formation between side groups is the first reaction to occur with an onset pressure near 9 GPa, as characterized using vibrational spectroscopy, X-ray diffraction, and computational studies. High-pressure reactivity is system-dependent and while functionalized arenes are predicted to exhibit reduced-barrier energy cycloaddition pathways, directed reactions between side groups can be used as a novel strategy for the formation unique polymeric materials.

The behavior of organic molecules under high-pressure conditions represents a developing field of chemical research. New reaction pathways become viable at elevated (GPa) pressures, leading to the formation of a variety of novel polymeric materials.[1, 2] Previous studies have shown a range of pressure-induced chemical reactions, such as free-radical polymerization,[3, 4] condensation reactions,[5] and Diels-Alder cycloadditions[6-19] are all viable at elevated pressures. Of particular interest are high-pressure reaction products rich in sp^3-bonded carbon that are predicted to possess remarkable mechanical,[20-25] thermal[26-28] and chemical stability,[29] making them possible candidates for a diverse range of applications.

Several recent studies have focused on π-stacked aromatic molecular precursors, which can react at high pressure via [4 + 2] cycloaddition[16, 17] to produce one-dimensional polymeric materials known as nanothreads.[6-19, 30-35] Nanothread formation can depend on hydrostatic vs. non-hydrostatic stress conditions, and precursors with parallel π-stacking, small slippage angles, and short interring distances tend to produce ordered nanothreads under rapid, hydrostatic compression.[12, 13, 18, 19, 31-36] Other aromatic crystals with offset stacking may also produce nanothreads, but typically require other factors such as anisotropic stress and slow compression to control reactivity (e.g., benzene,[6, 15] pyridine[7]). Thus, in the absence of polymorphic phase transitions that affect stacking, molecular crystals with minimally displaced π-stacking overlap may be screened as potential nanothread precursor candidates based on known crystal structures, or stacked systems may be designed though crystal engineering methods. In addition, the chemical homogeneity of resulting nanothreads may be improved using thread-directing groups that isolate selected cycloaddition pathways (e.g., pyridazine,[19] thiophene,[9] furan[8, 16, 17, 35]). Nevertheless, most nanothread formation reactions occur at pressures around 20 GPa,[6, 7, 11, 15, 32] which hinders large-volume scaling of these materials.

Several strategies to reduce nanothread reaction pressures have been employed including reducing aromaticity,[8, 17, 35] and utilizing external stimulus (e.g., heating,[37] photoexcitation[38]). For the case of molecular [4 + 2] cycloaddition reactions, it is well understood that the incorporation of electron withdrawing groups on the dieneophile and incorporation of donating

https://doi.org/10.26434/chemrxiv-2023-xsg7n **ORCID:** https://orcid.org/0000-0003-1011-8339 Content not peer-reviewed by ChemRxiv. **License:** CC BY-NC-ND 4.0

groups on the diene can promote reactions by reducing the HOMO-LUMO gap.[39] For example, cyano-substituted dienophiles in solution-phase Diels-Alder reactions have been shown to decrease the barrier to reaction by a factor of two, which increases reaction rates up to seven orders of magnitude.[40] Given the high reaction onset pressures required for nanothread formation, a crystal engineering strategy that allows one to incorporate a variety of functional groups with both electron withdrawing and donating character into precursors may potentially facilitate nanothread-forming reactions at lower pressures. Additionally, the incorporation of different functionalities may open avenues to polymeric materials with new and unusual structures and chemistries. Nevertheless, the incorporation of different functional groups may also enable alternative reaction pathways that could compete with nanothread-forming cycloaddition. Indeed, competing reactions between pendant groups has been shown for several systems containing disubstituted benzenes.[12] Additionally, functionalized nanothreads that retain some degree of sp^2 character may undergo post-synthetic tautomerization involving pendant groups and the nanothread backbone.[11] Thus, the interplay between functionalization-enhanced nanothread formation (e.g., via reduced-barrier cycloaddition) and the potential for new reaction pathways between functional groups must be examined to understand the roles of competing reaction pathways. In addition, targeted reactions between functional groups on molecular precursors could represent a new strategy to produce polymeric materials with unique structures and functionalities.

Charge-transfer cocrystals represent a promising class of nanothread precursors that can incorporate a wide range of functional groups. Partial charges between monomer stacking layers can provide sandwich-type p-stacking overlap with short interring distances that may enable controlled nanothread reactions at elevated pressures. Previous studies on arene:perfluoroarene cocrystals of benzene,[41] naphthalene[13, 14] and others[11] indicate the possibility for controlled nanothread formation, but reduced reaction pressures and enhanced thread homogeneity require improvements. Charge-transfer cocrystals may represent good candidates for the formation of nanothreads at reduced pressures. For example, cocrystals synthesized from 1,2,4,5-tetracyanobenzene (TCNB) form with considerable p overlap between aromatic rings along the stacking axis, and allow for the incorporation of a variety of electron withdrawing and donating groups (EWG/EDG), e.g., hexamethylbenzene,[42] *p*-hydroquinone,[43] and anthracene[44].

To further examine the role of electron withdrawing/donating groups on nanothread formation and the potential for competing reactions between side-groups, we studied the high-pressure behavior of a 1:1 cocrystal of 1,4-diaminobenzene (DAB) and 1,2,4,5-tetracyanobenzene (TCNB) using both theoretical calculations and experiments. Above 9 GPa, pedant amine (–NH_2) and cyano (–CN) groups react via nucleophilic attack to produce a new one-dimensional amidine-rich polymeric material. Further compression results in the formation of a chemically inhomogeneous product with evidence for the presence of sp^3-carbon. The results highlight a system-dependent balance between enhanced cycloaddition reactivity and side-group reactions and suggest a new strategy to produce novel polymeric materials via the controlled reaction of functional groups.

The published structure of the DAB:TCNB cocrystal[45] shows near-sandwich-type π-stacking with an average interring centroid distance of ~3.57 Å and average interring slippage angle of ~21°, making it an excellent candidate to undergo nanothread formation via sequential [4 + 2] Diels-Alder polymerization along the molecular stacking axis.[12] Based on known reactions at ambient pressure,[40] the incorporation of cyano-substituents on the ring may lower the reaction onset barrier and enable intermolecular [4 + 2] cycloaddition to occur at reduced pressures. To explore this possibility, we performed quantum chemical calculations to determine the reaction barriers and dimer energies for various [4 + 2] cycloadditions between DAB and TCNB rings (**Figure S1**). All reaction barriers for dimerization were found to be lower than that of benzene (55 kcal/mol) — nearly half the barrier energy in some cases (**Figure 1A**). These calculations suggest favorable reaction barriers for TCNB-DAB cycloaddition, however several similar interring distances (3.39 – 3.56 Å) and energy barriers for different pathways ($\Delta E^{\ddagger}$ = 31 – 35 kcal/mol) indicate that a single dominant nanothread-forming pathway is unlikely.

Interestingly, the crystal structure of DAB:TCNB also shows that the DAB rings are slightly tilted relative to the TCNB plane, which appears to be due to intermolecular interactions between amino groups and cyano groups in neighboring molecules within a stack (see **Figure 1B**). This tilt creates a short N···C separation of just 3.33 Å between amine (N) and cyano (C) groups, which is less than any of the interring distances in the low-barrier [4 + 2] cycloaddition reactions. Given the small distances between functional groups, we also calculated the relative energies of the dimers that would be formed by nucleophilic attack of a cyano group by an amine, followed by H-transfer to form an amidine. Note that due to the formation of a zwitterioninc transition state, calculation of a reaction barrier for this step was not possible (see SI). These dimers were found to be slightly lower in energy (ca. -5 kcal/mol) than the starting cocrystal (see **Figure S2**), indicating that amidine formation is exothermic and may potentially occur during the compression of DAB:TCNB. The DFT-optimized crystal structures of potential [4 + 2] nanothread and amidine polymers were found to be relatively close in energy compared to the starting cocrystal (+1.24 and -0.60 kcal/mol, respectively), suggesting that both reactions may be viable upon compression.

https://doi.org/10.26434/chemrxiv-2023-xsg7n **ORCID:** https://orcid.org/0000-0003-1011-8339 Content not peer-reviewed by ChemRxiv. **License:** CC BY-NC-ND 4.0

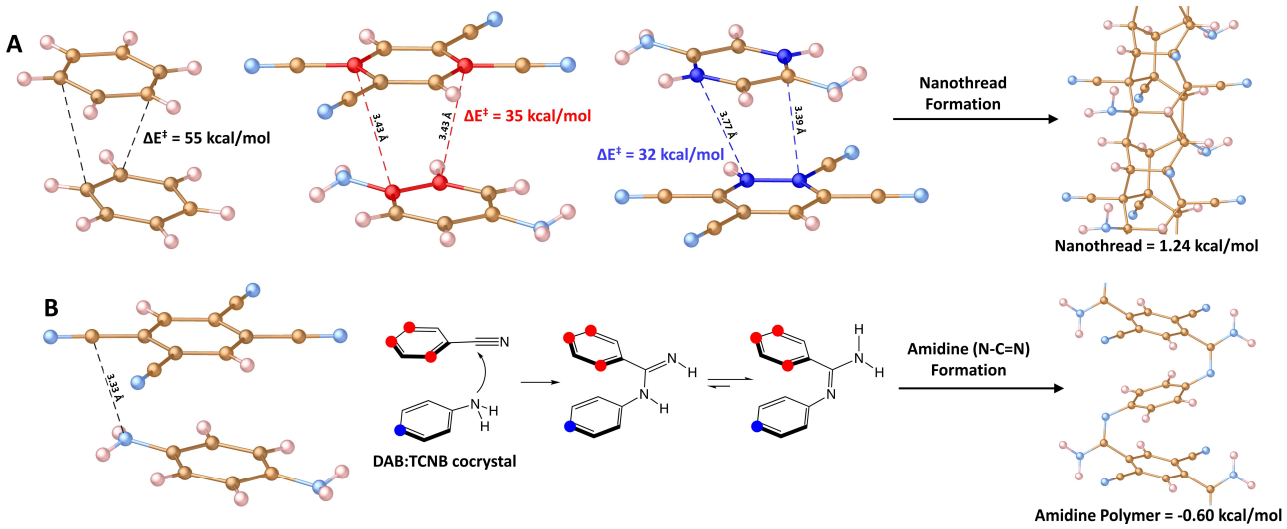

Figure 1. A) Comparison of the reaction barriers ($\Delta E^{\ddagger}$) for potential Diels-Alder [4 + 2] cycloaddition reactions in benzene and the DAB:TCNB cocrystal. Blue carbons represent reactions where DAB is acting as the diene, and red carbons represent reactions where TCNB is acting as the diene. $\Delta E^{\ddagger}$ values are determined for the gas phase energy of the transition states using DLPNO-CCSD(T) (see the **Supporting Information**). Right: Visualization and relative energy of a DFT-optimized crystalline nanothread structure formed by [4 + 2] cycloaddition. B) Closest-contact distances, formation mechanism, proposed structure, and relative energy of the resulting polymer for amidine formation between pendant -NH_2 and -CN groups in the DAB:TCNB cocrystal. Omitted -NH_2 and -CN groups are represented by blue and red dots, respectively. Energies of the crystalline structures are calculated relative to the starting DAB:TCNB cocrystal.

In order to examine the behavior of the cocrystal under pressure and determine the roles of cycloaddition vs. side-group reactions between monomer layers, a sample of DAB:TCNB (synthesized using the previously published method)[45] was loaded into a diamond-anvil cell (DAC) and monitored using a combination of in situ vibrational spectroscopy and X-ray diffraction (XRD).

Given that the vibrational properties of this cocrystal have not been reported, we calculated the infrared (IR) spectrum for DAB:TCNB to help assign vibrational modes and interpret changes in bonding with pressure (see **Figure S3** and **Table S1**). In situ FTIR measurements (**Figures 2A** and **S4**) indicate that above 5 GPa, N–H bending and stretching vibrations at 1624 cm^{-1} and 3459 cm^{-1} broaden significantly, and above 9 GPa, high-frequency shoulders emerge on both peaks. With increasing pressure, the intensity of the N–H stretching vibration decreases dramatically, disappearing almost entirely by 15 GPa. Interestingly, the disappearance of the N–H stretch is accompanied by a simultaneous decrease in intensity for C≡N vibrations at *ca*. 2250 cm^{-1} and the appearance of increased intensity around *ca*. 1600 cm^{-1}, consistent with new C=N vibrations.[46] Additionally, above 9 GPa, new peaks at *ca*. 1674, 1066, 1006, 742 and 711 cm^{-1} appear, further indicating the onset of a chemical reaction. Above 11 GPa, all FTIR peaks steadily broaden, and by 30 GPa no sharp peaks remain. In situ Raman spectra of the DAB:TCNB cocrystal were also collected over the same pressure range and show complementary changes to the FTIR spectra above 9 GPa (**Figure S5**), however, samples become sensitivity to laser irradiation at high pressure and exhibit radiation-induced damage.

In situ powder XRD data obtained during compression (**Figures 2B** and **S6**) are consistent with vibrational spectra. Upon compression, the Bragg peaks exhibit a monotonic shift to higher angles reflecting a contraction of the unit cell in response to increased pressure. Above 10 GPa, the relative intensities of the peaks corresponding to the $\{\bar{2}11\}$ and $\{\bar{2}21\}/\{040\}$ reflections begin to invert with the relative intensity of the $\{\bar{2}11\}$ peak increasing and the $\{\bar{2}21\}/\{040\}$ peak correspondingly decreasing in intensity. Above 20 GPa, the intensity of all Bragg peaks decreases further with minimal diffraction observed above 30 GPa, indicating a significant loss of crystallinity.

https://doi.org/10.26434/chemrxiv-2023-xsg7n **ORCID:** https://orcid.org/0000-0003-1011-8339 Content not peer-reviewed by ChemRxiv. **License:** CC BY-NC-ND 4.0

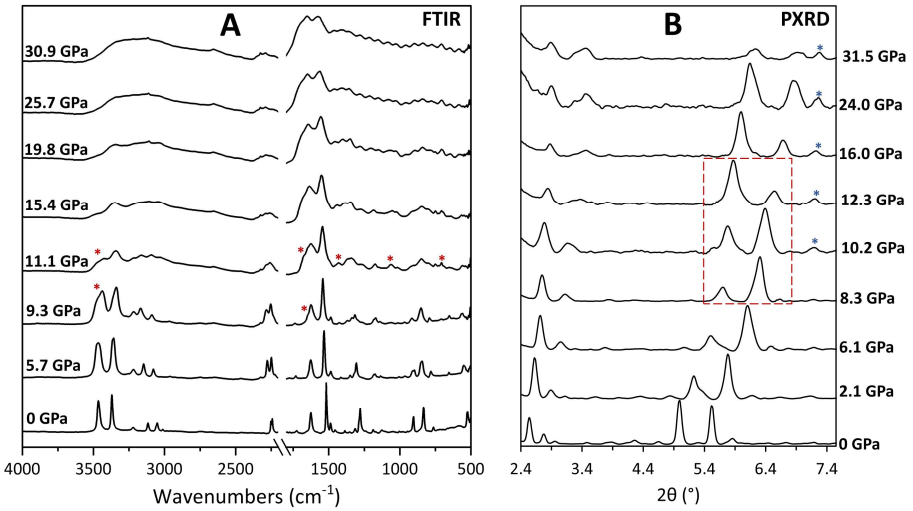

Figure 2. A) Variable-pressure FTIR absorption spectra for a DAB:TCNB cocrystal between 500 – 4000 cm^{-1} and 0 – 30.9 GPa. The diamond absorption region between 1800-2200 cm^{-1} has been omitted. Red asterisks indicate new peaks that appear above 9 GPa. B) In situ XRD patterns for DAB:TCNB (λ = 0.2952 Å) collected between 0 – 31.5 GPa. Red square indicates the intensity shift of the $\{\bar{2}11\}$ and $\{\bar{2}21\}/\{040\}$ reflections. Blue asterisks indicate diffraction from the rhenium gasket. Bragg peak intensity decreases gradually with pressure as can be observed by the relative increase in low-angle air scattering intensity at high pressure. All diffraction patterns are normalized to the most intense peak.

XRD patterns collected on the material recovered after decompression from ~30 GPa show that the sample remains partially crystalline, with a well-defined four-fold diffraction pattern clearly visible at *d* = 6.30 Å, and broad amorphous scattering is observed after background subtraction using an empty gasket hole (**Figure 3A**). The crystalline portion of the diffraction pattern of the recovered sample is consistent with the starting DAB:TCNB cocrystal when oriented along the stacking *c*-axis, which also exhibits four-fold diffraction corresponding to the {110} reflections at *d* = 6.80 Å at ambient conditions. The *d*-spacings of the {110} reflections in the recovered product are similar to those of the molecular cocrystal near the reaction onset pressure (6.27 Å at 8.3 GPa **Figure S7**). The similarity in *d*-spacings coupled with retention of the 4-fold diffraction suggests that the basic molecular packing of the precursors has been retained in the polymerized material, and that the crystalline component of the reaction proceeds such that the overall macromolecular geometry remains similar. Such behavior is consistent with previously reported topochemical-like reactions from cocrystal systems,[11-14] with a higher degree of disorder observed in the present case.

While the sample recovered from 30 GPa maintains some degree of crystallinity based on XRD, the FTIR spectrum consists of broad peaks indicating significant local chemical inhomogeneity (**Figure 3C**),[12] which is consistent with previous studies of functionalized benzenes and other nanothreads that possess crystalline macromolecular packing and a broad distribution of local chemical environments. Samples recovered from 30 GPa show clear evidence for the retention of starting functionality in the resulting material. Notably, the broad peak at *ca*. 2220 cm^{-1} (C≡N stretch, *cf.* 2242 cm^{-1} in TCNB) suggests retention of a fraction of the cyano groups, with an ~77% decrease in integrated peak intensity. The recovered product also shows a new, broad absorption feature at *ca*. 2900 cm^{-1} that may indicate the presence of sp^3 C–H vibrations, consistent with the formation of a disordered nanothread-like material via subsequent reactions of aromatic rings.

Given that chemical reactivity in compressed DAB:TCNB appears to occur in two stages, i.e., initial side-group reactivity near 9 GPa followed by further reactions at higher pressure, additional DAC samples were compressed to 15 GPa and recovered for characterization. This pressure was chosen as it is above the side-group reaction onset pressure, but below the pressure where significant broadening of the IR spectra and additional reactivity is observed. The FTIR spectrum of material recovered from 15 GPa confirms that the first reaction in DAB:TCNB occurs between pendant amino and cyano groups with the emergence of a new peaks at *ca*. 1649 cm^{-1} consistent with the formation of amidine C=N groups.[7, 19] Given the loss of N–H stretching vibrations at *ca.* 3461 cm^{-1}, and a significant decrease in intensity of the C≡N stretches at *ca*. 2242 and 2248 cm^{-1}, it is likely that these C=N groups are produced by the amidine-forming reaction shown in **Figure 1B**. While calculated barrier energies for reactions between pendant functional groups and adjacent aromatic rings are comparable to [4 + 2] cycloadditions between rings (**Figure S8**), large intermolecular distances (*i.e.,* >4 Å) likely prohibit such reactions and amidine formation appears to be the most probable explanation for the initial reaction near 9 GPa. Amidine formation via this reaction scheme is also supported by the loss of the DAB C–NH_2 vibration at *ca*. 1278 cm^{-1}, the emergence of a new amidine C–N vibration at *ca.* 1061 cm^{-1} (*cf.* 1061 cm^{-1} in imidazole[47]), and the presence of a new peak at *ca*. 3300 cm^{-1} consistent with sp^2 N–H

https://doi.org/10.26434/chemrxiv-2023-xsg7n **ORCID:** https://orcid.org/0000-0003-1011-8339 Content not peer-reviewed by ChemRxiv. **License:** CC BY-NC-ND 4.0

vibrations.[48] Furthermore, peaks corresponding to the sp^2 C–H stretching (>3000 cm^{-1}) and bending vibrations in DAB and TCNB (at *ca.* 833 cm^{-1} and 904 cm^{-1} respectively) remain present in the recovered sample, indicating that the core aromatic rings remain intact up to 15 GPa. Calculated FTIR spectra for four candidate polymer systems (see **Figure S9**) further supports the formation of an amidine rich polymer. Notably, the new peaks at *ca*. 1404 and 1379 cm^{-1} observed in the DAB:TCNB sample recovered after compression to 15 GPa can be assigned to C=N–C vibrations from the amidine group. The formation of the amidine polymer also explains the significant broadening of the peak at *ca*. 833 cm^{-1} in the starting cocrystal. Calculated FTIR of both amidine polymers shows several new peaks between 800-900 cm^{-1} which can be assigned to out-of-plane sp^2 C–H and N–H vibrations from the DAB and TCNB rings and the newly formed amidine group. Due to the broad FTIR spectrum for the sample recovered from 30 GPa, no clear assignment of a structure can be made.

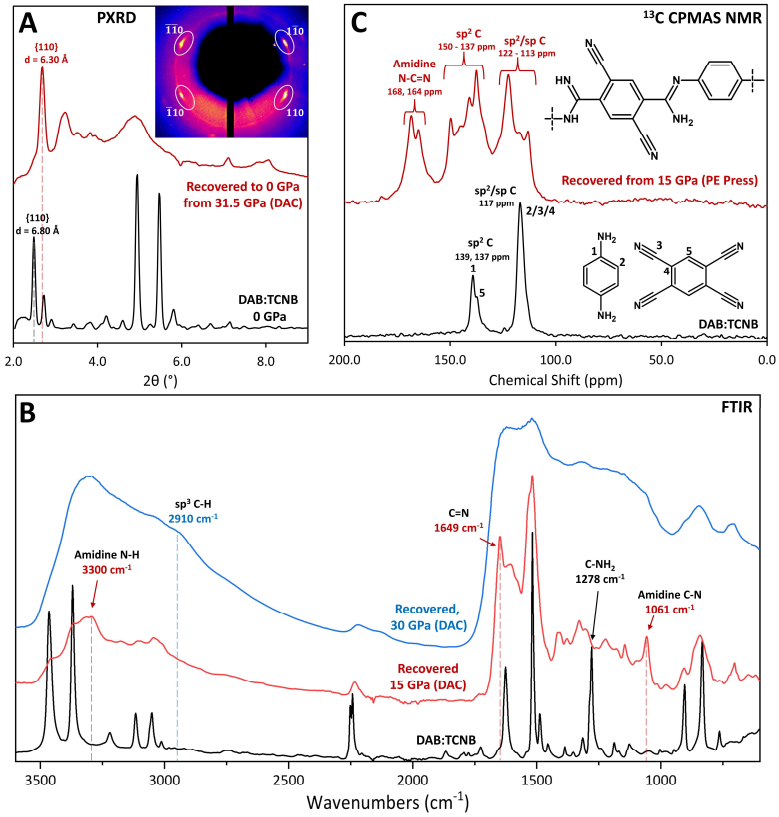

Figure 3. A) Comparison of the background-subtracted XRD patterns (λ = 0.2952 Å) for as-synthesized DAB:TCNB before (black) and after compression to 31.5 GPa (red). Inset: Two-dimensional diffraction pattern of the recovered sample collected at ambient conditions, showing a 4-fold diffraction pattern corresponding to the [49] reflections at *d* = 6.30 Å in the one-dimensional pattern. B) Comparison of FTIR spectra of molecular DAB:TCNB (black) and samples recovered to ambient conditions after compression to 15 (red) and 30 GPa (blue). C) ^{13}C Cross-polarized magic-angle spinning (CPMAS) NMR spectra for as-synthesized DAB:TCNB (black), and a PE press sample recovered from 15 GPa (red). Inset: Structures of the starting cocrystal and amidine polymer.

To enable additional characterization of the lower-pressure DAB:TCNB product phase, the synthesis of this material was scaled to mg quantities using a Paris-Edinburgh (PE) press (see **Materials and Methods**). The FTIR spectrum of the PE press sample recovered from ~15 GPa is in good agreement with the DAC sample recovered from the same pressure (**Figure S10**). Combined thermogravimetric analysis/differential scanning calorimetry (TGA/DSC) carried out on the recovered PE press sample supports the formation of an extended polymer via enhanced thermal stability (**Figure S11**). The starting molecular cocrystal shows a two-step decomposition process consistent with the behavior of previously reported TCNB cocrystals.[50] However, the recovered PE press sample remains thermally stable over this entire temperature range and does not decompose until >450 °C, aside from minor mass loss up to 100 °C, which is attributed to weakly absorbed water. The enhanced thermal stability of the recovered product clearly demonstrates a permanent pressure-induced chemical transformation resulting in the formation of a more thermally stable product.

Comparison of solid-state ^{13}C NMR spectra of the starting DAB:TCNB cocrystal and the product recovered from 15 GPa confirms the formation of an amidine-rich polymer upon compression (**Figure 3B**). The starting cocrystal exhibits three resolved

https://doi.org/10.26434/chemrxiv-2023-xsg7n **ORCID:** https://orcid.org/0000-0003-1011-8339 Content not peer-reviewed by ChemRxiv. **License:** CC BY-NC-ND 4.0

peaks at *ca*. 117, 137, and 139 ppm, consistent with the sp/sp^2 carbon environments of the constituent molecules. The ^{13}C NMR spectrum of the material recovered from 15 GPa is notably more complex than the starting material reflecting a distribution of chemical environments and loss of the starting molecular symmetry. Although it is difficult to precisely assign all specific contributions in the spectrum, overlapping peaks occupy three general frequency regions that provide valuable insights into the chemical nature of the product. Two groupings of peaks bracket the initial shifts in the molecular precursor (i.e., ~113–122 ppm, ~137–150 ppm), reflecting a distribution of sp/sp^2 carbons found in the molecular precursor. Notably, no carbon environments are observed at frequencies below *ca*. 113 ppm indicating no sp^3 carbon environments are formed during reaction, which confirms that no nanothread-forming cycloaddition reactions occur upon compression to 15 GPa. The third frequency range occurs between ~160–175 ppm. Compared with the starting cocrystal, two new peaks appear in the recovered product at *ca.* 164 and 168 ppm, which we assign to sp^2 amidine (N=C–N) environments, consistent with previous solid-state ^{13}C NMR studies of amidines.[51] This result confirms the proposed amidine reaction scheme shown in **Figure 1B**. The presence of two amidine peaks can be explained by the presence of both HN=C–NH and H_2N–C=N amidines. Materials containing amidine groups are important for their diverse chemical and pharmacological properties. Notably, photoluminescent amidine-rich polymers have been used to selectively detect and capture metal cations and as fluorescent probes in biological imaging.[52] However, formation of amidine-rich materials is challenging. One-step synthesis of amidines from reaction between amines and cyano groups is only possible if the C≡N groups are activated through the incorporation of electron withdrawing species (e.g., CF_3CN)[53] or by the use of Lewis acid catalysts.[54] Formation of amidine-rich polymers is an especially difficult multicomponent reaction process that must be carried out under inert conditions.[52, 55] Therefore, solid-state compression represents a novel route to obtain amidine rich polymers using a simple process.

In summary, this work demonstrates that tetracyanobenzene charge transfer cocrystals can be used as a platform for the high-pressure formation of polymeric materials under compression. Theoretical calculations predict that the incorporation of electron donating and withdrawing groups in these cocrystals can significantly lower the energy barrier associated with nanothread-forming [4 + 2] cycloaddition reactions compared to non-functionalized analogues, suggesting that optimized functionalization could reduce the onset pressures required for nanothread formation. Nevertheless, interactions between specific pendant functional groups are also important as new side-group reactions may become favorable leading to entirely new reaction pathways. For the case of DAB:TCNB, the initial polymerization mechanism indeed occurs between pendant side groups through the formation of an amidine polymer, while the formation of sp^3 carbon between core aromatic rings may occur at higher pressures. Similar to nanothreads, the new amidine-rich product is a one-dimensional polymer that packs with chains along the molecular stacking axis in a paracrystalline product. Unlike nanothreads, the amidine product has one bond in each direction and is thus more like a conventional polymer. Similar to many nanothread products, the observed crystallinity of the amidine originates from the macromolecular packing of chains that individually have some chemical heterogeneity. Side-chain polymerization between functional groups represents a new method to be explored further for controlled solid-state reactions. Directed side-chain polymerization reactions may serve as a new method to create novel polymeric materials with functionalities and bonding motifs that are difficult to obtain through conventional approaches.

ASSOCIATED CONTENT

Supporting Information

Supporting information contains additional experimental procedures, Figures S1–S11, and Table S1.

AUTHOR INFORMATION

Corresponding Authors

Samuel G. Dunning - Earth and Planets Laboratory, Carnegie Institution for Science, Washington, District of Columbia 20015, United States
Email: sdunning@carnegiescience.edu
Timothy A. Strobel - Earth and Planets Laboratory, Carnegie Institution for Science, Washington, District of Columbia 20015, United States
Email: tstrobel@carnegiescience.edu

ORCID

Samuel G. Dunning: 0000-0003-1011-8339
Wan Si Tang: 0000-0002-7893-3025
Li Zhu: 0000-0001-8588-9379
Bo Chen: 0000-0002-5084-1321
George D. Cody: 0000-0003-4176-3648
Stella Chariton: 0000-0001-5522-0498

https://doi.org/10.26434/chemrxiv-2023-xsg7n **ORCID:** https://orcid.org/0000-0003-1011-8339 Content not peer-reviewed by ChemRxiv. **License:** CC BY-NC-ND 4.0

Vitali B. Prakapenka: 0000-0001-9270-2330
Timothy A. Strobel: 0000-0003-0338-4380

Present Addresses

⊥ Electrochemical Safety Research Institute, UL Research Institutes, Houston, TX 77204, United States

Author Contributions

The manuscript was written through contributions of all authors. All authors have given approval to the final version of the manuscript.

Notes

The authors declare no competing financial interests.

ACKNOWLEDGMENTS

Portions of this work were performed at GeoSoilEnviroCARS (The University of Chicago, Sector 13), Advanced Photon Source (APS), Argonne National Laboratory. GeoSoilEnviroCARS is supported by the National Science Foundation – Earth Sciences (EAR – 1634415). This research used resources of the Advanced Photon Source, a U.S. Department of Energy (DOE) Office of Science User Facility operated for the DOE Office of Science by Argonne National Laboratory under Contract No. DE-AC02-06CH11357.

The authors acknowledge funding support from The Arnold and Mabel Beckman Foundation (Arnold O. Beckman Postdoctoral Fellowship in Chemical Sciences Program) and the U.S. Army Research Office (Grant W911NF-17-1-0604). B.C. acknowledges the financial support from MCIN/AEI/10.13039/501100011033/FEDER, UE (project PID2021-123573NA-I00).

REFERENCES

1. Li, F.; Xu, J.; Wang, Y.; Zheng, H.; Li, K., Pressure-Induced Polymerization: Addition and Condensation Reactions. *Molecules* **2021,** *26* (24), 7581.
2. Yoo, C.-S., Chemistry under extreme conditions: Pressure evolution of chemical bonding and structure in dense solids. *Matter Rad. Extremes* **2020,** *5* (1), 018202.
3. Sun, J.; Dong, X.; Wang, Y.; Li, K.; Zheng, H.; Wang, L.; Cody, G. D.; Tulk, C. A.; Molaison, J. J.; Lin, X.; Meng, Y.; Jin, C.; Mao, H.-k., Pressure-Induced Polymerization of Acetylene: Structure-Directed Stereoselectivity and a Possible Route to Graphane. *Angew. Chem. Int. Ed.* **2017,** *56* (23), 6553-6557.
4. Han, J.; Tang, X.; Wang, Y.; Wang, Y.; Han, Y.; Lin, X.; Dong, X.; Lee, H. H.; Zheng, H.; Li, K.; Mao, H.-k., Pressure-Induced Polymerization of Monosodium Acetylide: A Radical Reaction Initiated Topochemically. *J. Phys. Chem. C* **2019,** *123* (50), 30746-30753.
5. Zheng, H.; Li, K.; Cody, G. D.; Tulk, C. A.; Dong, X.; Gao, G.; Molaison, J. J.; Liu, Z.; Feygenson, M.; Yang, W.; Ivanov, I. N.; Basile, L.; Idrobo, J.-C.; Guthrie, M.; Mao, H.-k., Polymerization of Acetonitrile via a Hydrogen Transfer Reaction from CH_3 to CN under Extreme Conditions. *Angew. Chem. Int. Ed.* **2016,** *55* (39), 12040-12044.
6. Fitzgibbons, T. C.; Guthrie, M.; Xu, E. S.; Crespi, V. H.; Davidowski, S. K.; Cody, G. D.; Alem, N.; Badding, J. V., Benzene-derived carbon nanothreads. *Nat. Mater.* **2015,** *14* (1), 43-47.
7. Li, X.; Wang, T.; Duan, P.; Baldini, M.; Huang, H. T.; Chen, B.; Juhl, S. J.; Koeplinger, D.; Crespi, V. H.; Schmidt-Rohr, K.; Hoffmann, R.; Alem, N.; Guthrie, M.; Zhang, X.; Badding, J. V., Carbon Nitride Nanothread Crystals Derived from Pyridine. *J. Am. Chem. Soc.* **2018,** *140* (15), 4969-4972.
8. Huss, S.; Wu, S. K.; Chen, B.; Wang, T.; Gerthoffer, M. C.; Ryan, D. J.; Smith, S. E.; Crespi, V. H.; Badding, J. V.; Elacqua, E., Scalable Synthesis of Crystalline One-Dimensional Carbon Nanothreads through Modest-Pressure Polymerization of Furan. *ACS Nano* **2021,** *15* (3), 4134-4143.
9. Biswas, A.; Ward, M. D.; Wang, T.; Zhu, L.; Huang, H.-T.; Badding, J. V.; Crespi, V. H.; Strobel, T. A., Evidence for Orientational Order in Nanothreads Derived from Thiophene. *J. Phys. Chem. Lett.* **2019,** *10* (22), 7164-7171.
10. Nobrega, M. M.; Teixeira-Neto, E.; Cairns, A. B.; Temperini, M. L. A.; Bini, R., One-dimensional diamondoid polyaniline-like nanothreads from compressed crystal aniline. *Chem. Sci.* **2018,** *9* (1), 254-260.
11. Gerthoffer, M. C.; Wu, S. K.; Chen, B.; Wang, T.; Huss, S.; Oburn, S. M.; Crespi, V. H.; Badding, J. V.; Elacqua, E., 'Sacrificial' supramolecular assembly and pressure-induced polymerization: toward sequence-defined functionalized nanothreads. *Chem. Sci.* **2020,** *11* (42), 11419-11424.
12. Tang, W. S.; Strobel, T. A., Evidence for Functionalized Carbon Nanothreads from pi-Stacked, para-Disubstituted Benzenes. *J. Phys. Chem. C* **2020,** *124* (45), 25062-25070.

https://doi.org/10.26434/chemrxiv-2023-xsg7n **ORCID:** https://orcid.org/0000-0003-1011-8339 Content not peer-reviewed by ChemRxiv. **License:** CC BY-NC-ND 4.0

13. Ward, M. D.; Tang, W. S.; Zhu, L.; Popov, D.; Cody, G. D.; Strobel, T. A., Controlled Single-Crystalline Polymerization of $C_{10}H_8{\cdot}C_{10}F_8$ under Pressure. *Macromolecules* **2019,** *52* (20), 7557-7563.
14. Friedrich, A.; Collings, I. E.; Dziubek, K. F.; Fanetti, S.; Radacki, K.; Ruiz-Fuertes, J.; Pellicer-Porres, J.; Hanfland, M.; Sieh, D.; Bini, R.; Clark, S. J.; Marder, T. B., Pressure-Induced Polymerization of Polycyclic Arene-Perfluoroarene Cocrystals: Single Crystal X-ray Diffraction Studies, Reaction Kinetics, and Design of Columnar Hydrofluorocarbons. *J. Am. Chem. Soc.* **2020,** *142* (44), 18907-18923.
15. Li, X.; Baldin, M.; Wang, T.; Chen, B.; Xu, E. S.; Vermilyea, B.; Crespi, V. H.; Hoffmann, R.; Molaison, J. J.; Tulk, C. A.; Guthrie, M.; Sinogeikin, S.; Badding, J. V., Mechanochemical Synthesis of Carbon Nanothread Single Crystals. *J. Am. Chem. Soc.* **2017,** *139* (45), 16343-16349.
16. Matsuura, B. S.; Huss, S.; Zheng, Z. X.; Yuan, S. C.; Wang, T.; Chen, B.; Badding, J. V.; Trauner, D.; Elacqua, E.; van Duin, A. C. T.; Crespi, V. H.; Schmidt-Rohr, K., Perfect and Defective ^{13}C-Furan-Derived Nanothreads from Modest Pressure Synthesis Analyzed by ^{13}C NMR. *J. Am. Chem. Soc.* **2021,** *143* (25), 9529-9542.
17. Dunning, S. G.; Chen, B.; Zhu, L.; Cody, G. D.; Chariton, S.; Prakapenka, V. B.; Zhang, D.; Strobel, T. A., Synthesis and Post-Processing of Chemically Homogeneous Nanothreads from 2,5-Furandicarboxylic Acid. *Angew. Chem. Int. Ed.* **2023,** *62* (14), e202217023.
18. Romi, S.; Fanetti, S.; Alabarse, F.; Bini, R., Structure–Reactivity Relationship in the High-Pressure Formation of Double-Core Carbon Nanothreads from Azobenzene Crystal. *J. Phys. Chem. C* **2021,** *125* (31), 17174-17182.
19. Dunning, S. G.; Zhu, L.; Chen, B.; Chariton, S.; Prakapenka, V. B.; Somayazulu, M.; Strobel, T. A., Solid-State Pathway Control via Reaction-Directing Heteroatoms: Ordered Pyridazine Nanothreads through Selective Cycloaddition. *J. Am. Chem. Soc.* **2022,** *144* (5), 2073-2078.
20. Demingos, P. G.; Muniz, A. R., Electronic and Mechanical Properties of Partially Saturated Carbon and Carbon Nitride Nanothreads. *J. Phys. Chem. C* **2019,** *123* (6), 3886-3891.
21. Demingos, P. G.; Balzaretti, N. M.; Muniz, A. R., First-principles study of carbon nanothreads derived from five-membered heterocyclic rings: thiophene, furan and pyrrole. *Phys. Chem. Chem. Phys.* **2021,** *23* (3), 2055-2062.
22. Roman, R. E.; Kwan, K.; Cranford, S. W., Mechanical Properties and Defect Sensitivity of Diamond Nanothreads. *Nano. Lett.* **2015,** *15* (3), 1585-1590.
23. Silveira, J.; Muniz, A. R., First-principles calculation of the mechanical properties of diamond nanothreads. *Carbon* **2017,** *113*, 260-265.
24. Zheng, Z. Q.; Zhan, H. F.; Nie, Y. H.; Xu, X.; Gu, Y. T., Role of Nitrogen on the Mechanical Properties of the Novel Carbon Nitride Nanothreads. *J. Phys. Chem. C* **2019,** *123* (47), 28977-28984.
25. Silveira, J.; Muniz, A. R., Diamond nanothread-based 2D and 3D materials: Diamond nanomeshes and nanofoams. *Carbon* **2018,** *139*, 789-800.
26. Zhan, H. F.; Gu, Y. T., Thermal Conductivity of Diamond Nanothread. In *Thermal Transport in Carbon-Based Nanomaterials*, Zhang, G., Ed. Elsevier: 2017; pp 185-204.
27. Zhan, H. F.; Gu, Y. T., Thermal conduction of one-dimensional carbon nanomaterials and nanoarchitectures. *Chinese Phys. B* **2018,** *27* (3), 038103.
28. Zhan, H. F.; Zhang, G.; Zhang, Y. Y.; Tan, V. B. C.; Bell, J. M.; Gu, Y. T., Thermal conductivity of a new carbon nanotube analog: The diamond nanothread. *Carbon* **2016,** *98*, 232-237.
29. Saha, B.; Pratik, S. M.; Datta, A., Coexistence of Normal and Auxetic Behavior in a Thermally and Chemically Stable sp^3 Nanothread: Poly 5 asterane. *Chem.-Eur. J.* **2017,** *23* (52), 12917-12923.
30. Xu, E.-s.; Lammert, P. E.; Crespi, V. H., Systematic Enumeration of sp^3 Nanothreads. *Nano. Lett.* **2015,** *15* (8), 5124-5130.
31. Li, Y. P.; Tang, X. Y.; Zhang, P. J.; Wang, Y. D.; Yang, X.; Wang, X.; Li, K.; Wang, Y. J.; Wu, N. N.; Tang, M. X.; Xiang, J. F.; Lin, X. H.; Lee, H. H.; Dong, X.; Zheng, H. Y.; Mao, H. K., Scalable High-Pressure Synthesis of sp2-sp3 Carbon Nanoribbon via [4 + 2] Polymerization of 1,3,5-Triethynylbenzene. *J. Phys. Chem. Lett.* **2021,** *12* (30), 7140-7145.
32. Romi, S.; Fanetti, S.; Alabarse, F. G.; Bini, R.; Santoro, M., High-Pressure Synthesis of 1D Low-Bandgap Polymers Embedded in Diamond-like Carbon Nanothreads. *Chem. Mater.* **2022,** *34* (5), 2422-2428.
33. Romi, S.; Fanetti, S.; Alabarse, F.; Mio, A. M.; Haines, J.; Bini, R., Towards custom built double core carbon nanothreads using stilbene and pseudo-stilbene type systems. *Nanoscale* **2022,** *14* (12), 4614-4625.
34. Romi, S.; Fanetti, S.; Alabarse, F.; Mio, A. M.; Bini, R., Synthesis of double core chromophore-functionalized nanothreads by compressing azobenzene in a diamond anvil cell. *Chem. Sci.* **2021,** *12* (20), 7048-7057.
35. Wang, X.; Yang, X.; Wang, Y.; Tang, X.; Zheng, H.; Zhang, P.; Gao, D.; Che, G.; Wang, Z.; Guan, A.; Xiang, J.-F.; Tang, M.; Dong, X.; Li, K.; Mao, H.-k., From Biomass to Functional Crystalline Diamond Nanothread: Pressure-Induced Polymerization of 2,5-Furandicarboxylic Acid. *J. Am. Chem. Soc.* **2022,** *144* (48), 21837-21842.
36. Gao, D.; Tang, X.; Xu, J.; Yang, X.; Zhang, P.; Che, G.; Wang, Y.; Chen, Y.; Gao, X.; Dong, X.; Zheng, H.; Li, K.; Mao, H.-k., Crystalline $C_3N_3H_3$ tube (3,0) nanothreads. *PNAS* **2022,** *119* (17), e2201165119.

https://doi.org/10.26434/chemrxiv-2023-xsg7n **ORCID:** https://orcid.org/0000-0003-1011-8339 Content not peer-reviewed by ChemRxiv. **License:** CC BY-NC-ND 4.0

37. Fanetti, S.; Santoro, M.; Alabarse, F.; Enrico, B.; Bini, R., Modulating the H-bond strength by varying the temperature for the high pressure synthesis of nitrogen rich carbon nanothreads. *Nanoscale* **2020,** *12* (8), 5233-5242.
38. Oburn, S. M.; Huss, S.; Cox, J.; Gerthoffer, M. C.; Wu, S.; Biswas, A.; Murphy, M.; Crespi, V. H.; Badding, J. V.; Lopez, S. A.; Elacqua, E., Photochemically Mediated Polymerization of Molecular Furan and Pyridine: Synthesis of Nanothreads at Reduced Pressures. *J. Am. Chem. Soc.* **2022,** *144* (48), 22026-22034.
39. Houk, K. N., Generalized Frontier Orbitals of Alkenes and Dienes - Regioselectivity in Diels-Alder Reactions. *J. Am. Chem. Soc.* **1973,** *95* (12), 4092-4094.
40. Tang, S.-Y.; Shi, J.; Guo, Q.-X., Accurate prediction of rate constants of Diels–Alder reactions and application to design of Diels–Alder ligation. *Org. Biomol. Chem.* **2012,** *10* (13), 2673-2682.
41. Wang, Y.; Dong, X.; Tang, X.; Zheng, H.; Li, K.; Lin, X.; Fang, L.; Sun, G. a.; Chen, X.; Xie, L.; Bull, C. L.; Funnell, N. P.; Hattori, T.; Sano-Furukawa, A.; Chen, J.; Hensley, D. K.; Cody, G. D.; Ren, Y.; Lee, H. H.; Mao, H.-k., Pressure-Induced Diels–Alder Reactions in C_6H_6-C_6F_6 Cocrystal towards Graphane Structure. *Angew. Chem. Int. Ed.* **2019,** *58* (5), 1468-1473.
42. Saraswatula, V. G.; Sharada, D.; Saha, B. K., Stronger π···π Interaction Leads to a Smaller Thermal Expansion in Some Charge Transfer Complexes. *Cryst. Growth Des.* **2018,** *18* (1), 52-56.
43. Bock, H.; Seitz, W.; Sievert, M.; Kleine, M.; Bats, J. W., Donor/acceptor complexes between hydroquinone, pyrene, perylene, and N,N,N',N'-tetramethylbenzidine with 1,2,4,5-tetracyanobenzene or tetracyanohydroquinone: Structures with and without H bridge networks. *Liebigs Ann.* **1996,** (11), 1929-1940.
44. Stezowski, J. J., Crystal-Structure of a Low-Temperature Phase of the 1-1 Charge-Transfer Complex Between Anthracene and Tetracyanobenzene. *J. Phys. Chem.* **1979,** *83* (4), 550-551.
45. Tsuchiya, H.; Marumo, F.; Saito, Y., The crystal structure of the 1:1 complex of p-phenylenediamine and 1,2,4,5-tetracyanobenzene. *Acta Crystallogr. B* **1973,** *B 29* (APR15), 659-666.
46. Barkakaty, B.; Browning, K. L.; Sumpter, B.; Uhrig, D.; Karpisova, I.; Harman, K. W.; Ivanov, I.; Hensley, D. K.; Messman, J. M.; Kilbey, S. M., II; Lokitz, B. S., Amidine-Functionalized Poly(2-vinyl-4,4-dimethylazlactone) for Selective and Efficient CO2 Fixing. *Macromolecules* **2016,** *49* (5), 1523-1531.
47. Van Bael, M. K.; Smets, J.; Schoone, K.; Houben, L.; McCarthy, W.; Adamowicz, L.; Nowak, M. J.; Maes, G., Matrix-Isolation FTIR Studies and Theoretical Calculations of Hydrogen-Bonded Complexes of Imidazole. A Comparison between Experimental Results and Different Calculation Methods. *J. Phys. Chem. A* **1997,** *101* (13), 2397-2413.
48. Grivas, J. C.; Taurins, A., Infrared Spectra – Structure Correlations of N-Substituted Trifluoroacetamidines. *Can. J. Chem.* **1961,** *39* (3), 414-419.
49. Giordano, N.; Beavers, C. M.; Campbell, B. J.; Eigner, V.; Gregoryanz, E.; Marshall, W. G.; Pena-Alvarez, M.; Teat, S. J.; Vennari, C. E.; Parsons, S., High-pressure polymorphism in pyridine. *IUCrJ* **2020,** *7* (1), 58-70.
50. Bawa, A. S.; Meunier-Prest, R.; Rousselin, Y.; Couvercelle, J. P.; Stern, C.; Malzieux, B.; Bouvet, M., Series of charge transfer complexes obtained as crystals in a confined environment. *CrystEngComm* **2021,** *23* (36), 6418-6426.
51. Pereira, F. S.; Lincon da Silva Agostini, D.; do Espírito Santo, R. D.; deAzevedo, E. R.; Bonagamba, T. J.; Job, A. E.; González, E. R. P., A comparative solid state ^{13}C NMR and thermal study of CO_2 capture by amidines PMDBD and DBN. *Green Chem.* **2011,** *13* (8), 2146-2153.
52. Su, X.; Han, T.; Niu, N.; Li, H.; Wang, D.; Tang, B. Z., Facile Multicomponent Polymerizations toward Multifunctional Heterochain Polymers with α,β-Unsaturated Amidines. *Macromolecules* **2021,** *54* (21), 9906-9918.
53. Grivas, J. C.; Taurins, A., Further Studies on the Reaction Between Halogen-Substituted Nitriles and Amines. *Can. J. Chem.* **1961,** *39* (4), 761-764.
54. Wang, J.; Xu, F.; Cai, T.; Shen, Q., Addition of Amines to Nitriles Catalyzed by Ytterbium Amides: An Efficient One-Step Synthesis of Monosubstituted N-Arylamidines. *Org. Lett.* **2008,** *10* (3), 445-448.
55. Lee, I.-H.; Kim, H.; Choi, T.-L., Cu-Catalyzed Multicomponent Polymerization To Synthesize a Library of Poly(N-sulfonylamidines). *J. Am. Chem. Soc.* **2013,** *135* (10), 3760-3763.

https://doi.org/10.26434/chemrxiv-2023-xsg7n **ORCID:** https://orcid.org/0000-0003-1011-8339 Content not peer-reviewed by ChemRxiv. **License:** CC BY-NC-ND 4.0